Theoretical and Applied Mechanics Letters 15 (2025) 100614

Contents lists available at ScienceDirect

Theoretical and Applied Mechanics Letters

journal homepage: www.elsevier.com/locate/taml

Research Article

Randomly adjustable stacked open thin-shell cells mechanical metamaterials

Xiaolin Guo[a,b], Bohua Sun[b,c,d,*]

[a] School of Civil Engineering & Institute of Mechanics and Technology, Xi'an University of Architecture and Technology, Xi'an 710055, China
[b] Beijing Key Laboratory of High-Entropy Energy Materials and Devices, Beijing Institute of Nanoenergy and Nanosystems, Chinese Academy of Sciences, Beijing 101400, China
[c] School of Nanoscience and Engineering, University of Chinese Academy of Sciences, Beijing 100049, China
[d] School of Sciences & Institute of Mechanics and Technology, Xi'an University of Architecture and Technology, Xi'an 710055, China

ARTICLE INFO

Keywords:
Open thin-shell
Mechanical metamaterials
Randomly
Energy absorption

ABSTRACT

Open thin-shell structures exhibit advantages such as lightweight properties and high energy absorption efficiency. By randomly stacking these structures as unit cells, adjustable mechanical metamaterials with tunable and stable mechanical properties can be constructed. This study investigates the mechanical performance of randomly stacked open thin-shell mechanical metamaterials using a combined experimental and numerical simulation approach. Results indicate that under compressive loading, shell unit cells primarily dissipate energy through large deformation, snap-fit behavior, friction, and shell relocation. Different combinations of randomly stacked mechanical metamaterials demonstrate nearly identical energy dissipation ratios during the first compression-unloading cycle, indicating that the energy dissipation efficiency exhibits robust stability independent of contact and geometric randomness. However, under limit cycle conditions, increasing the proportion of Type II shells enhances the maximum relative displacement, energy dissipation capacity, and energy dissipation ratio by up to fivefold. Notably, under compressive loading, Type I shells engaged through snap-fit behavior exhibit irreversible deformation after unloading, while Type II shells maintain their configuration without active engagement. The proportion of Type II shells directly determines the mechanical performance of the structure.This research provides new references for the development of lightweight mechanical metamaterials, disordered mechanical metamaterials, and adjustable mechanical metamaterials.

1. Introduction

Metamaterials are artificially designed materials that subvert the conventional paradigm of material property regulation. By innovatively controlling and exploiting physical mechanisms, they achieve extraordinary performance unattainable in natural materials. The unique properties of metamaterials primarily originate from sophisticated geometric designs [1–3], rather than the intrinsic attributes of constituent materials. In recent years, mechanical metamaterials have garnered significant attention due to their distinctive mechanical characteristics, including multistable configurations [4,5], tunable stiffness [6,7], negative Poisson's ratio [8,9], and negative thermal expansion [10]. These characteristics can be achieved through the design of metamaterials.

The adjustability of metamaterials refers to the phenomenon where desired mechanical properties emerge as functions of controllable parameters, such as geometric parameters, boundary conditions, and external constraints [11]. Current research recognizes shape-reconfigurable systems leveraging structural instabilities or structural deformation as effective approaches for achieving tunability and programmability in mechanical metamaterials [12,13]. For instance, conventional materials absorb energy through irreversible plastic deformation [14–16], whereas adjustable mechanical metamaterials primarily utilize mechanical instabilities in deformable microstructures for energy absorption [17]. Building upon this characteristic, researchers are actively exploring metamaterial design strategies incorporating compliant Structures buckling [18,19], hinged multi-segment structures [20,21], and structural locking [22–24].

In the design of mechanical metamaterials, thin-walled structures (e.g., rods, plates, shells) have gradually become key components due to their advantages of lightweight properties and high energy absorption efficiency. During axial compression, these structures utilize their inherent bending and buckling mechanisms to convert external energy into stored bending energy. Upon removal of the external load, the stored energy is released. The traditional "buckliphobia" toward struc-

* Corresponding author.
E-mail address: sunbohua@binn.cas.cn (B. Sun).

https://doi.org/10.1016/j.taml.2025.100614
Received 11 July 2025; Received in revised form 4 September 2025; Accepted 4 September 2025
Available online 12 September 2025

tures has transformed into “buckliphilia” with such mechanical instabilities being regarded as mechanical energy transducers [25]. Meanwhile, researchers have investigated the tunable mechanical properties of elastic thin-walled structures, including friction/torsion/buckling of elastic strips [26–28], snap-fit behavior of elastic shells [29–32], and indentation of elastic arches on frictional substrates [33]. However, current studies remain focused on individual thin-walled structures. For composite systems formed by stacking multiple thin-walled structures, their potential to generate more complex and predictable mechanical responses through interactions between units has not been fully explored.

Indeed, research on the stacking of thin structures has a long history: in 1992, Poirier et al. [34] conducted pioneering research on the localized deformation of stacked closed cylindrical thin shells. This seminal work proposed three types of disordered stacking configurations: contact disorder, geometric disorder, and compositional disorder. Poirier’s study specifically focused on contact disorder, examining the behavior of identical cylinders (with identical geometry and material composition) under uniaxial compression. Subsequent developments include Poincloux et al. [35] analyzing the bending response of stacked thin sheets (book-like structures), and Sun et al. [36] investigating energy dissipation through interlayer sliding in layered systems. Recently, inspired by disordered microstructures in biological materials (e.g., spider silk, bone tissue), researchers have begun exploring the influence of structural disorder on metamaterial performance [37–39], marking a paradigm shift from traditionally ordered architectures to controlled-disorder engineering in advanced material design. In 2023, Sano et al. [40] proposed a mechanical energy absorber composed of randomly stacked identical open cylindrical shells, which functions as a adjustable mechanical metamaterial ingeniously integrated with shell-shell snap-fit. Through combined experimental and two-dimensional (2D) simulation approaches, they demonstrated that the stacked shells can absorb and store mechanical energy during compression. Despite the random stacking configuration of shells, the system exhibited statistically robust mechanical performance. These studies on stacked slender structures reveal that the rearrangement of thin-shell cellular units (flexible components) can generate versatile and predictable mechanical responses. However, existing studies on randomly stacked mechanical metamaterials based on thin-shell unit cells have only considered the contact disorder of shells with identical openings, and their research has primarily focused on the mechanical properties under the first compression load. Thus, further investigations are still required.

This study uses open cylindrical thin shells as unit cells to design 42 types of randomly stacked mechanical metamaterials with thin shells of different openings, introducing geometric disorder on the basis of contact disorder (including positional disorder), thus not limited to shells with identical openings. The thin-shell unit cells were fabricated using the PET thermoplastic molding process, and the mechanical metamaterials were formed by randomly stacking different thin-shell unit cells under gravity. First, the mechanical properties and energy dissipation of two thin-shell unit cells under compressive loading were analyzed. Building on this, the deformation processes of different combinations of randomly stacked thin-shell mechanical metamaterials under compressive loading, as well as their characteristics and mechanical properties under cyclic loading, were further investigated, with a particular focus on comparing the mechanical properties between the first and tenth loading cycles. The influence of the opening angle Φ of the thin-shell unit cells on the stiffness and energy dissipation capacity of these randomly stacked mechanical metamaterials under cyclic loading (specifically the first and tenth cycles) was analyzed. Additionally, finite element analysis software ABAQUS was used to construct three-dimensional mechanical metamaterials by randomly stacking open thin-shell unit cells, and numerical simulations of the cyclic compression-unloading process were performed. Experimental results were combined to validate the correctness of the model. This research is highly likely to fill the gap in the field regarding the design of aperiodic randomly stacked unit cell metamaterials and mechanical property research under cyclic compression loading, providing new references for the study of lightweight, disordered, and adjustable mechanical metamaterials.

2. Design and fabrication

This study is based on the fundamental principles of dissipate energy through thin-shell bending deformation, snap-fit, friction, and shell relocation. By using $N = 30$ open cylindrical thin-shells as unit cells and randomly stacking them (disordered arrangement) under gravity within U-shaped containers, various mechanical metamaterials were designed, as shown in Fig. 1. The containers are made of acrylic plates with internal dimensions of 200 mm × 300 mm × 12 mm. The open cylindrical thin-shells have a radius $R = 19$ mm, an opening angle Φ in the range $1.75\ \text{rad} \le \Phi \le 3.1\ \text{rad}$, and a thickness $t = 0.42$ mm. The open cylindrical thin-shells are fabricated via a thermoforming process using polyethylene terephthalate (PET). The density of the PET material is $\rho = 1.35\ \text{g·cm}^{-3}$, and its Poisson’s ratio is $\nu = 0.35$. Transparent PET sheets with a thickness of 0.42 mm are cut into straight strips using a guillotine shear, with a width $b = 10$ mm and a length L in the range $66.6\ \text{mm} \le L \le 119.3\ \text{mm}$. The surfaces of the strips are lightly polished with sandpaper to prevent adhesion. A thermoforming mold is designed and fabricated by 3D printing aluminum alloy, and the straight strips are inserted into the reserved gaps in the mold to uniformly bend them into open cylindrical thin-shells with a curvature radius of 19 mm. The strips and mold are heated in an 85 °C water bath for 10 min, then removed and cooled in tap water (15 °C–20 °C) for 5 min for demolding. The entire fabrication process of the open cylindrical thin-shell unit cells is shown in Fig. 2.

Considering the effects of gravity and external forces, the stacked system exhibits a phenomenon where one open shell is driven to snap-fit with another. Under compression, open thin-shells display “snap-fit” behavior, which can be classified into two types based on the motion of the upper shell: Type I snap-fit (sliding engagement of the upper shell with the lower shell) and Type II snap-fit (snapping motion of the upper shell to engage the lower shell). As established by Yoshida et al. [29] and Guo et al. [30–32], the snap-fit type is governed by the friction coefficient μ and the opening angle Φ. In this study, all open cylindrical shells share identical radii (eliminating geometric misfit), and with a constant friction coefficient μ, the analysis focuses solely on the role of the opening angle Φ.

We selected shells with Type I opening angles $\Phi_1 = 1.75$ rad, $\Phi_2 = 2.1$ rad, and $\Phi_3 = 2.36$ rad and shells with Type II opening angles $\Phi_4 = 2.7$ rad, $\Phi_5 = 2.88$ rad, and $\Phi_6 = 3.05$ rad for investigation. To achieve geometric disorder by considering the disordered composition of randomly stacked open thin-shell mechanical metamaterials, we mixed shells with different opening angles (combining Type I and Type II shells). Therefore, Φ_1 shells were separately combined with Φ_4, Φ_5, and Φ_6 shells in six ratios (Type A = 30:0, Type B = 24:6, Type C = 18:12, Type D = 12:18, Type E = 6:24, Type F = 0:30) and named accordingly; for example, Φ_{1-4} Type C represents a random stacking combination of Φ_1 shells (18 units) and Φ_4 shells (12 units). Similarly, Φ_2 shells were combined with Φ_4, Φ_5, and Φ_6 shells; Φ_3 shells were combined with Φ_4, Φ_5, and Φ_6 shells, all in six ratios. As shown in Fig. 3, the randomly stacked open thin-shell mechanical metamaterials are illustrated, with their initial height before compression recorded as H_0.

3. Experimental

3.1. Material characterization

Material characterization of the open thin-shells was conducted, and the obtained material properties were applied to finite element simulations to simulate the compression-unloading cyclic testing process of three-dimensional (3D) randomly stacked open thin-shell mechanical metamaterials.

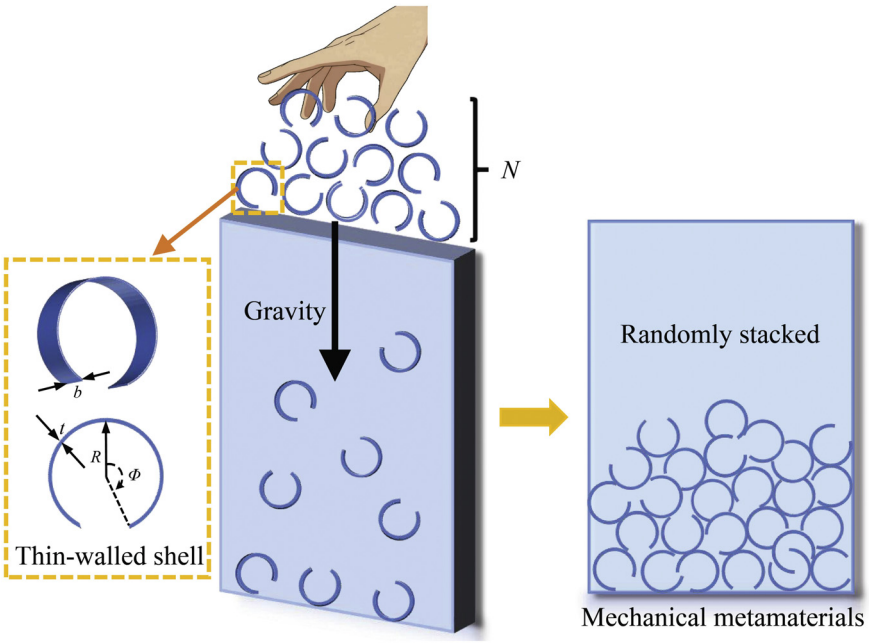

Fig. 1. Schematic of randomly stacked open thin-shell mechanical metamaterials.

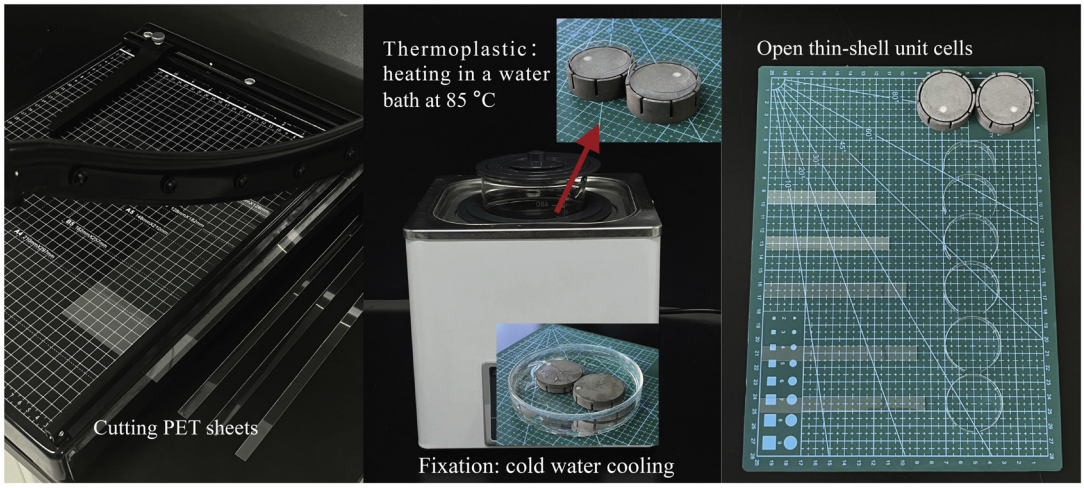

Fig. 2. Fabrication process of open cylindrical thin-shell unit cells.

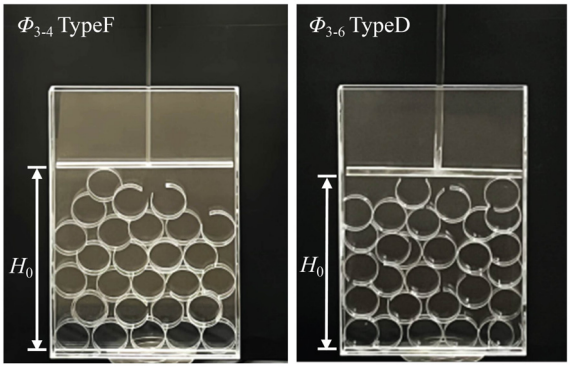

Fig. 3. Randomly stacked open thin-shells mechanical metamaterials.

Following the GB13022-91 standard *Test Method for Tensile Properties of Plastic Films* (which references the international standard ISO 1184–1983), strip-shaped tensile specimens were prepared. This method is applicable to plastic sheets with thicknesses less than 1 mm. The PET sheets used in the experiments had a thickness of 0.42 mm, with two layers of transparent protective films (which were removed during testing). The specimens were cut using a guillotine shear, and the experimental setup and specimen dimensions for tensile testing are shown in Fig. 4(a). Quasi-static isothermal tensile tests were performed using a universal testing machine (MTS) at a loading rate of 5 mm·min^{-3}. The nominal stress-nominal strain curves obtained from the tests are shown in Fig. 4(b). These curves were converted into true stress-true strain relationships to derive the fundamental material property parameters. As shown in Fig. 4(b), at small strains (near the origin region), stress increases approximately linearly with strain, exhibiting a linear elastic behavior consistent with Hooke's law; during this stage, material deformation is fully recoverable, corresponding to the elastic stage. When the strain exceeds a critical value, the stress-strain curve deviates from linearity and enters a nonlinear deformation region, where the material begins to exhibit irreversible plastic deformation. With further strain increase, stress continues to rise, showing strain hardening behavior—the

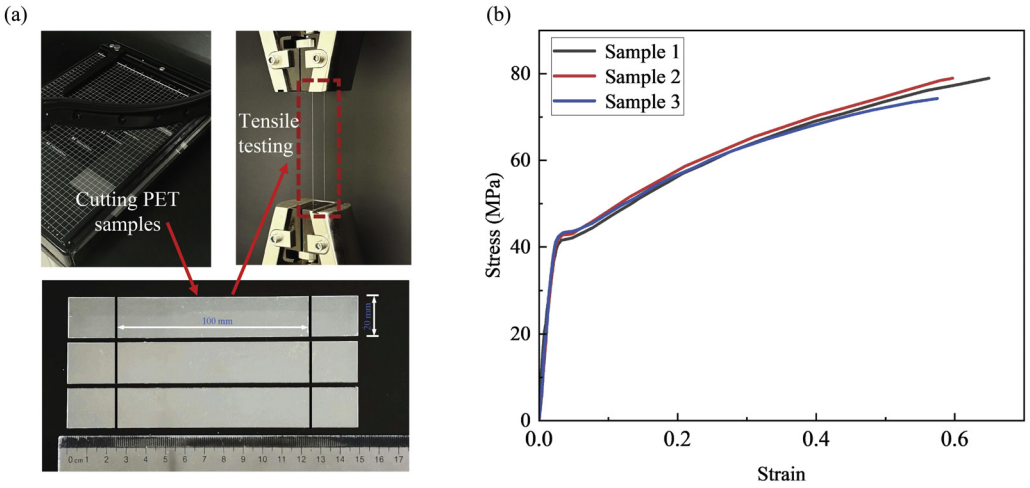

Fig. 4. (a) Tensile specimens and experimental setup; (b) stress-strain curves of the tensile specimens.

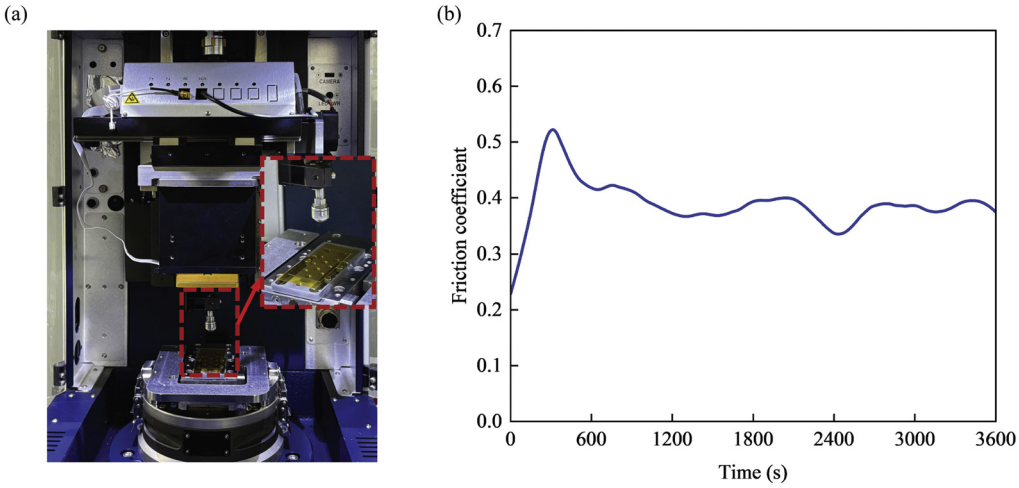

Fig. 5. (a) Friction and wear specimens and testing equipment; (b) friction curve.

material's resistance to deformation increases with accumulating plastic strain. The results of this mechanical property test are consistent with the characteristics of elastoplastic materials.

The coefficient of friction is an important property of materials, reflecting the friction characteristics between material surfaces. Dry friction tests were performed using a Bruker UMT Tribolab tribometer with a ball-on-disc contact configuration. Since PET sheets cannot be directly fabricated into small spherical samples, a 5 mm diameter metal ball was used, coated with a 0.05 mm thick PET film. The lower sample was a 0.42 mm thick PET sheet. The normal load was set at 1 N, the sliding stroke at 1 mm, the sliding frequency at 3 Hz, and the test duration was 60 min. As shown in Fig. 5, the friction coefficient curve of the PET sheet was obtained after the friction and wear experiment.

3.2. Compression snap-fit testing of two open thin-shells

To better design the combinations of open thin-shells within the structure and comprehensively understand the mechanical properties and deformation processes of stacked shells, prior to conducting random stacking experiments with different combinations of open thin-shells, we performed pairwise engagement testing on cylindrical thin-shells with varying Φ. Tests were established by attaching acrylic plates inside/outside the open thin-shelled structures and using MTS. The lower shell was fixed, while the upper shell was displaced downward at a speed of 2 mm·s^{-1}. The upper part of the shell was connected to the universal testing machine to measure the assembly force f and displacement u throughout the process, as shown in Fig. 6.

3.3. Cyclic compression testing of randomly stacked open thin-shells mechanical metamaterials

To evaluate the mechanical properties of different combinations of randomly stacked open thin-shell mechanical metamaterials, we conducted cyclic compression-unloading tests using MTS at room temperature, as shown in Fig. 7. To ensure that the thin-shell deformation remained within the elastic regime and that snap-fit occurred during compression, the maximum force applied by the upper rigid plate was controlled at $F_{max} = 5$ N throughout the cyclic compression testing process.

First, 30 open thin-shells were randomly stacked under gravity within the container according to different combinations, with the rigid plate suspended at the initial height H_0. The upper end of the rigid plate was connected to the load cell of the universal testing machine without contacting the container walls. The universal testing machine was then programmed to execute a cyclic compression-unloading testing protocol: when the maximum force applied by the upper rigid plate reached 5 N, it immediately retracted to the initial position H_0. This cycle was repeated 10 times per group. During this process, the compressive displacement of the stacked thin-shells is defined as $\Delta = H_0 - H$, where H represents the height of the stacked thin-shells during compression. In

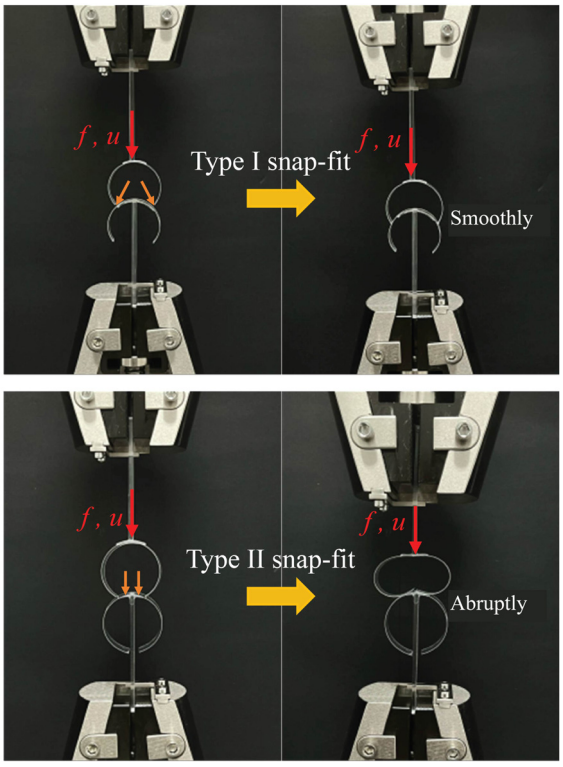

Fig. 6. Compression snap-fit testing of two open thin-shells.

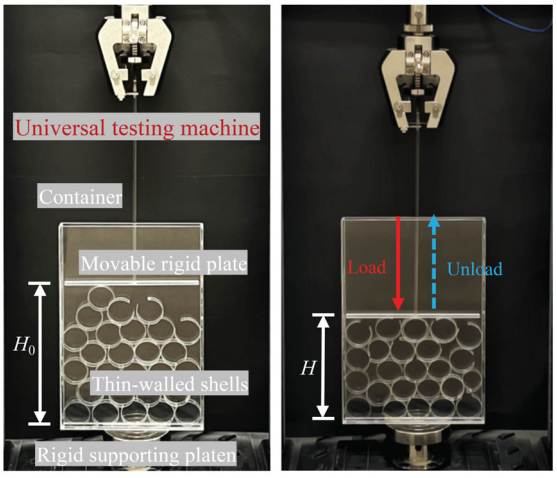

Fig. 7. Cyclic compression-unloading testing.

each cycle, when the force applied by the rigid plate reaches $F = F_{\max} = 5\,\mathrm{N}$, the compressive displacement attains its maximum value $\Delta_{\max}$. To ensure the generality of experimental results, 30 replicate tests (including 30 randomized stacking configurations and corresponding 30 sets of compression-unloading cyclic tests) were performed for each combination of randomly stacked open thin-shells mechanical metamaterials. The data acquisition system of the equipment precisely recorded the entire testing process, with the force-displacement ($F-\Delta$) curves captured via built-in sensors in the universal testing machine.

4. Numerical simulation

Three-dimensional numerical simulations were performed using ABAQUS to investigate the compression snap-fit process of two open thin-shells, as well as the deformation processes, cyclic characteristics, and mechanical properties of randomly stacked open thin-shells mechanical metamaterials with different combinations. The explicit dynamics solver of the software was employed to effectively address structural nonlinearities, large deformations, and complex contact interactions.

4.1. Compression snap-fit simulation of two open thin-shells

The Abaqus/Explicit general solver module was employed. The input parameters of the finite element model adopt the PET material model, with the relevant material parameters detailed in the Sections 2 and 3. The model setup reflects the experimental apparatus. To simulate the experimental conditions, the open thin-shell is bonded to a rectangular rigid body (inside/outside) to measure the installation force f and displacement u during the compression process. The in-plane longitudinal direction of the finite element model is the Y-direction, and the in-plane transverse direction is the X-direction. The finite element model is illustrated in Fig. 8(a). Throughout the simulation, the rigid body tied to the upper open thin-shell was prescribed a constant velocity along the Y-direction while all other degrees of freedom were constrained, whereas the rigid body tied to the lower open thin-shell remained fixed. To prevent interpenetration between open thin-shells, the model's contact was defined as general contact with "hard" normal contact behavior, and the system friction coefficient μ was varied between 0 and 0.5. The three-dimensional shell element type S4R was used, with free meshing generating quadrilateral elements. A mesh convergence study was conducted, selecting a global element size of 1 mm for numerical simulations considering computational accuracy, as shown in Fig. 8(b).

Finite element model validation was performed by simulating the compression snap-fit of two identical open elastic thin-shells under varying μ. Assuming the upper and lower open elastic thin-shells are precisely contact-fixed, the boundary conditions between Type I snap-fit and Type II snap-fit for the two elastic thin-shells at this state can be derived according to the analytical boundary formula provided by Yoshida and Wada [29] for distinguishing Type I and Type II snap-fit:

$$\frac{\frac{1}{2}-\cos(\Phi)\cdot\left(-1+\Phi\sin(\Phi)+\frac{3}{2}\cos(\Phi)\right)}{\frac{1}{2}-\cos(\Phi)\cdot\left(\frac{3\sin(\Phi)}{2}-\Phi\cos(\Phi)\right)}+\frac{\tan(\Phi)-\mu}{1+\mu\tan(\Phi)}=0. \tag{1}$$

Determine the critical angle $\Phi^*(\mu)$ for Type I and Type II snap-fit. As shown in Fig. 9, the simulation results of snap-fit between the two thin-shells under compression exhibit strong agreement with the snap-fit classification in the contact mechanics framework established by Yoshida and Wada.

When the upper and lower open elastic thin-shells are identical, the relationship between the μ, Φ, and snap-fit type aligns with the results from Sano et al. [40] 2D compression simulations of elastic double shells, thereby demonstrating the validity of the finite element model.

4.2. Cyclic compression simulation of randomly stacked open thin-shells mechanical metamaterials

The Abaqus/Explicit general solver module was employed. The material parameters of the open thin-shells adopt the PET material model, and the container is modeled as a U-shaped rigid shell. To avoid interpenetration between stacked shell unit cells, the model's contact is defined as general contact with "hard" behavior in the normal direction. Based on friction experiments and the relationship between the friction coefficient μ, opening angle Φ, and snap-fit type, the friction coefficient μ is set to 0.35. The three-dimensional shell element type S4R is used, with quadrilateral elements generated via free meshing; a global element size of 1 mm is selected for the numerical simulations. First, 30 shell unit cells of different combinations were randomly stacked under gravity, with constraints allowing only translational motion along the X/Y directions and rotational motion about the Z-axis. The stacked

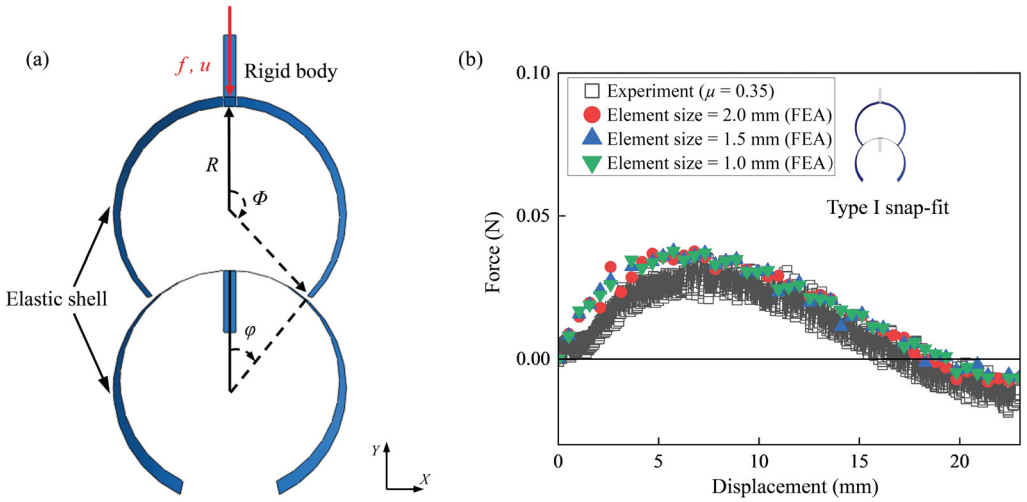

Fig. 8. (a) Finite element model of two open cylindrical thin-shells. (b) Force-displacement curves for different mesh sizes.

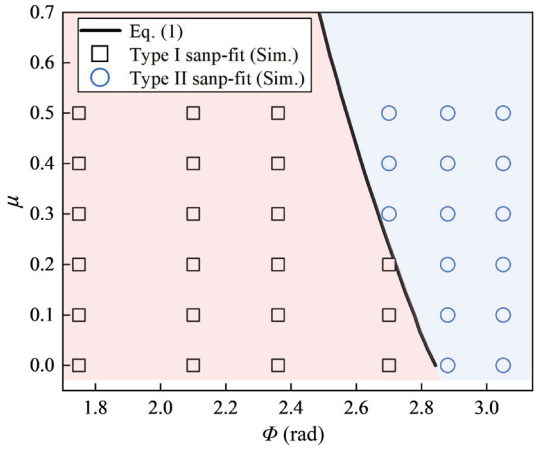

Fig. 9. Phase diagram of snap-fit deformation modes for two identical open cylindrical thin-shells.

unit cells and container were then imported into a new model as initial parts for assembly, with a rectangular rigid shell positioned above the unit cells without contacting the container. The compression process was configured with the upper rectangular rigid shell moving at a constant velocity along the *Y*-direction, while all other degrees of freedom were constrained. The unit cells were permitted only to translate along the *X*/*Y* directions and rotate about the *Z*-axis, with a gravity field applied throughout the system. A termination criterion was defined in the analysis step: the *Y*-direction reaction force from the rigid plate must not exceed 5 N, and the analysis terminates once this preset condition is met, consistent with the experimental setup where the rigid plate's $F_{max} = 5$ N. The displacement at termination corresponds to Δ_{max} of the first cycle. Subsequently, the rigid plate was retracted to the initial position H_0 (unloading phase). The result of the first unloading was then used as the starting point for the second compression, maintaining the rigid plate's initial position. This procedure was repeated cyclically to capture the complete compression-unloading process for each cycle. The establishment of this finite element model is divided into two main steps: the first step involves random stacking under gravity, and the second step conducts cyclic compression-unloading loading. The complete process of the finite element model establishment is illustrated in Fig. 10.

Integrating the experimental results from this study with the findings of Sano et al. [40], open cylindrical thin-shells with opening angles Φ_1, Φ_2, Φ_3, Φ_4, Φ_5, and Φ_6 were randomly stacked and assembled into six groups of mechanical metamaterials with identical open thin-shell unit cells. These groups were selected as validation cases to verify the correctness of the finite element model.

First, we validate the finite element model for the random stacking under gravity in the first step. The H_0 of the randomly stacked open thin-shells increases with the Φ and ultimately reaches a limit height (i.e., when $\Phi \to \pi$). Based on the hexagonal close packing (HCP) demonstrated by Norwegian mathematician Thue [41] as the most efficient planar packing arrangement, it can be derived that as $\Phi \to \pi$, the H_0 of 30 randomly stacked identical shell unit cells approaches $R(2+6\sqrt{3})$, neglecting the shell thickness. As shown in Fig. 11, our simulations of random stacking under gravity show that the normalized initial height H_0/R aligns with both experimental results and HCP predictions.

Next, we validate the finite element model for the second step of cyclic compression-unloading loading. The force-displacement curves from the first compression-unloading cycle in both numerical simulations and experiments are compared, with the F normalized by R^2/B (where B is the bending modulus of the shell), as shown in Fig. 12. The numerical simulation results demonstrate good agreement with the experimental results.

5. Results and discussion

5.1. Compression snap-fit study of two open thin-shells

Experimental results were comparatively validated against finite element simulations. Based on friction experiments and the relationship between the μ, Φ, and snap-fit type, the friction coefficient was set to $\mu = 0.35$. The snap-fit type between the two open thin-shells is primarily governed by both μ and Φ. However, with uniform material properties and a constant μ maintained in this study, the snap-fit type is solely determined by the Φ.

For Type I snap-fit, the upper shell with $\Phi_3 = 2.36$ rad was selected, while for Type II snap-fit, the upper shell with $\Phi_4 = 2.7$ rad was chosen. As shown in Fig. 13, the force-displacement curves of Type I and Type II open thin-shells are plotted, with the force f normalized by R^2/B. It is evident that the force required for Type II snap-fit significantly exceeds that of Type I snap-fit, i.e., $f_{\text{Type II}} \gg f_{\text{Type I}}$. As shown in Fig. 8, when the contact angle between the upper and lower shells satisfies $\phi = \Phi - \pi/2$, the edge of the upper shell tightly engages with the lower shell. For Type I snap-fit, as the assembly force f increases, the opening of the upper shell gradually expands. Through sliding, spontaneous snap-fit with the lower shell occurs under a negative force condition

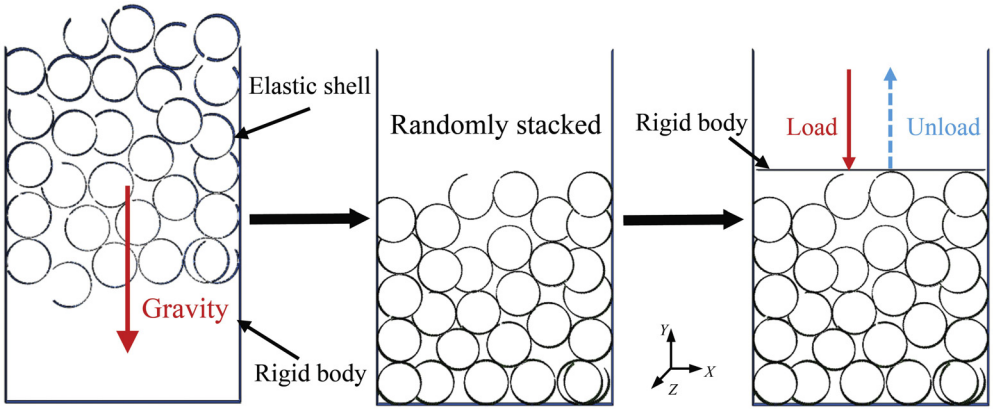

Fig. 10. Full Process of finite element modeling for randomly stacked open thin-shells mechanical metamaterials.

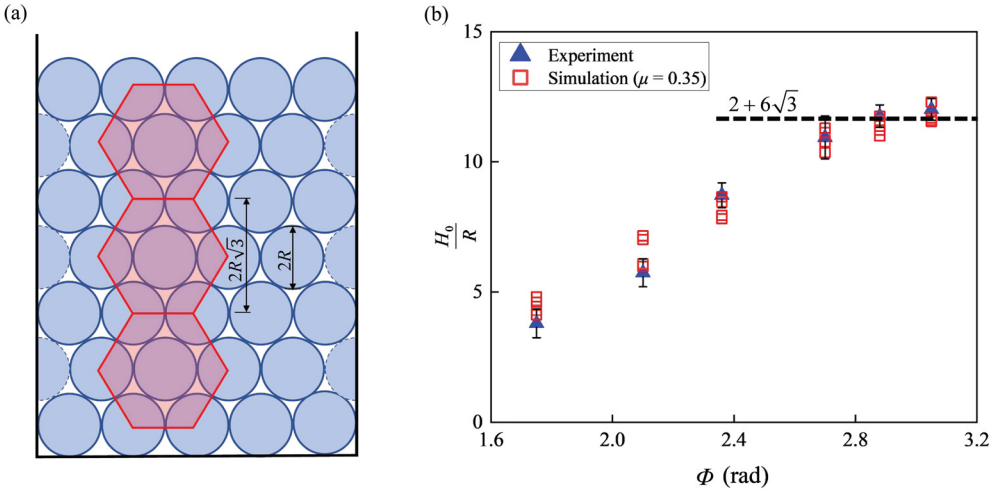

Fig. 11. (a) In-plane hexagonal close packing (HCP) of circular units. (b) Relationship between initial height H_0 and opening angle Φ (Data are presented as mean ±SD , $n = 30$).

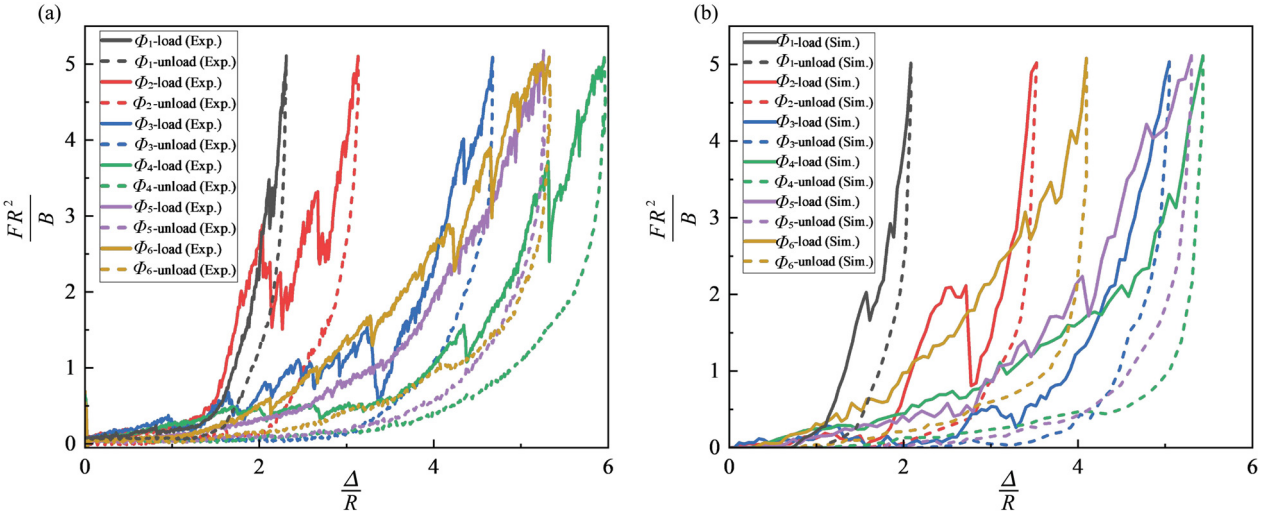

Fig. 12. $F - \Delta$ curves of mechanical metamaterials composed of randomly stacked identical open thin-shell unit cells.

($f < 0$). In contrast, for Type II snap-fit, increasing the assembly force f induces large deformations in the upper shell. When the indentation depth reaches a critical threshold, sudden snapping occurs, accompanied by a discontinuous force jump. The numerical simulations of the entire snap-fit process demonstrate strong agreement with experimental results.

To better understand the mechanical behavior of open thin-shells under external loading for different snap-fit types, we investigated the energy dissipation during the assembly process, defining the energy dissipation during assembly as E_A,

$$E_A = \int_0^u |f(u)|\,\mathrm{d}u. \tag{2}$$

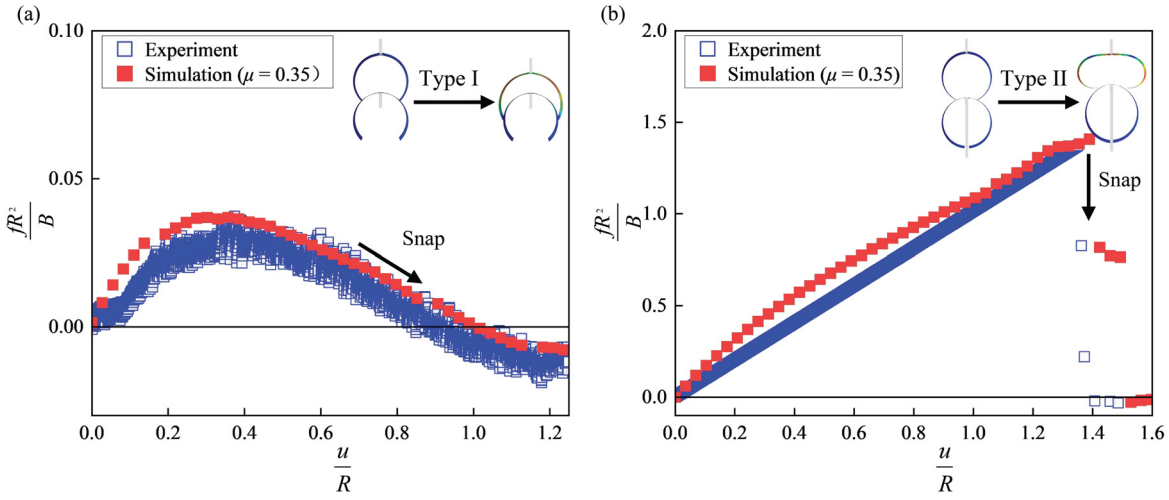

Fig. 13. Force-displacement curves for Type I and Type II open thin-shells snap-fit.

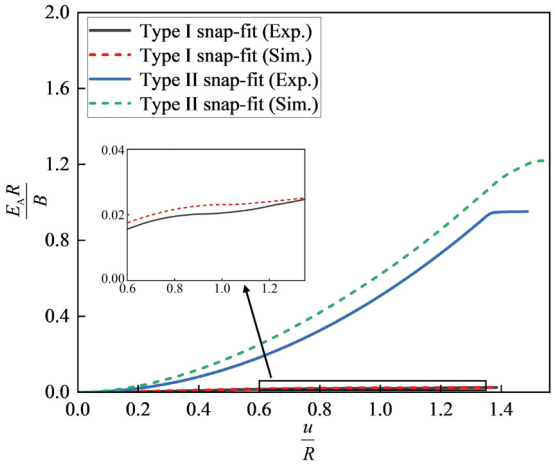

Fig. 14. Energy dissipation during the two thin-shells snap-fit process.

A normalized analysis was conducted on the energy dissipation during the snap-fit process of the two shells. The energy dissipation in Type II snap-fit far exceeds that of Type I, with $E_{\text{A-Type II}}$ being approximately 40 to 50 times greater than $E_{\text{A-Type I}}$, as shown in Fig. 14. Notably, the energy dissipation in Type II snap-fit increases nearly exponentially before reaching the critical snap-fit force. Based on these findings, we propose that mechanical metamaterials composed of randomly stacked Type II open thin-shells would exhibit superior energy absorption properties.

5.2. Deformation process of randomly stacked open thin-shells mechanical metamaterials under compressive loading

By investigating the deformation processes of randomly stacked open thin-shell mechanical metamaterials under compressive loading, the structural stability and reliability can be better evaluated. In this study, 42 types of randomly stacked mechanical metamaterials were designed, which can be categorized into three major groups: (1) mechanical metamaterials composed of randomly stacked identical Type I open thin-shells, (2) mechanical metamaterials composed of randomly stacked identical Type II open thin-shells, and (3) mechanical metamaterials composed of mixed random stacking of Type I and Type II open thin-shells.

Comparison of experimental and finite element simulation results. Although the initial conditions of experiments and simulations are difficult to be completely identical, leading to minor discrepancies in the deformation processes, their variation patterns exhibit strong consistency, as shown in Figs. 15–17.

Figure 15 shows the deformation processes of experiments and simulations for mechanical metamaterials composed of randomly stacked identical Type I open thin-shells. Under compressive loading, the open thin-shells mutually compress, undergoing snap-fit, elastic bending, and movement to resist compression, with the snap-fit process being irreversible. After the stacking of shell unit cells, stiffness enhancement occurs, leading to an increase in the overall structural stiffness. Dissipate energy throughout the process relies on shells' snap-fit, elastic deformation, friction, and repositioning.

Figure 16 shows the deformation processes of experiments and simulations for mechanical metamaterials composed of randomly stacked identical Type II open thin-shells. Under compressive loading, Type II open thin-shells lack sufficient space for snap-fit. The shell unit cells can only resist compression through elastic bending and movement. As illustrated, the deformation of Type II shell unit cells under compression can be viewed as resembling the digit '6', indicating that the overall structure exhibits superior flexibility to withstand compressive loads. In densely packed configurations, compressive loading can only induce elastic deformation and repositioning in Type II open thin-shells. Dissipate energy throughout the process relies on shells' elastic deformation, friction, and repositioning.

Figure 17 shows the deformation processes of experiments and simulations for mechanical metamaterials composed of mixed random stacking of Type I and Type II open thin-shells. Under compressive loading, Type I open thin-shells engage with surrounding shells through snap-fit, while resisting compression via elastic bending and movement, with the snap-fit process being irreversible. Simultaneously, Type II open thin-shells passively engage with Type I shells through snap-fit resisting compression via elastic bending and friction. After stacking the shell unit cells, stiffness enhancement occurs, leading to increased overall structural stiffness. Dissipate energy throughout the process relies on shells' snap-fit, elastic deformation, friction, and repositioning.

5.3. Cyclic characteristics of randomly stacked open thin-shells mechanical metamaterials under cyclic loading

We conducted an in-depth analysis of the cyclic characteristics of randomly stacked open thin-shells mechanical metamaterials with different compositional types under cyclic compression-unloading loading. Three sample groups—Φ_{3-6} Type A, Φ_{3-6} Type F, and Φ_{3-6} Type D—were selected for investigation. Due to the inherently random stack-

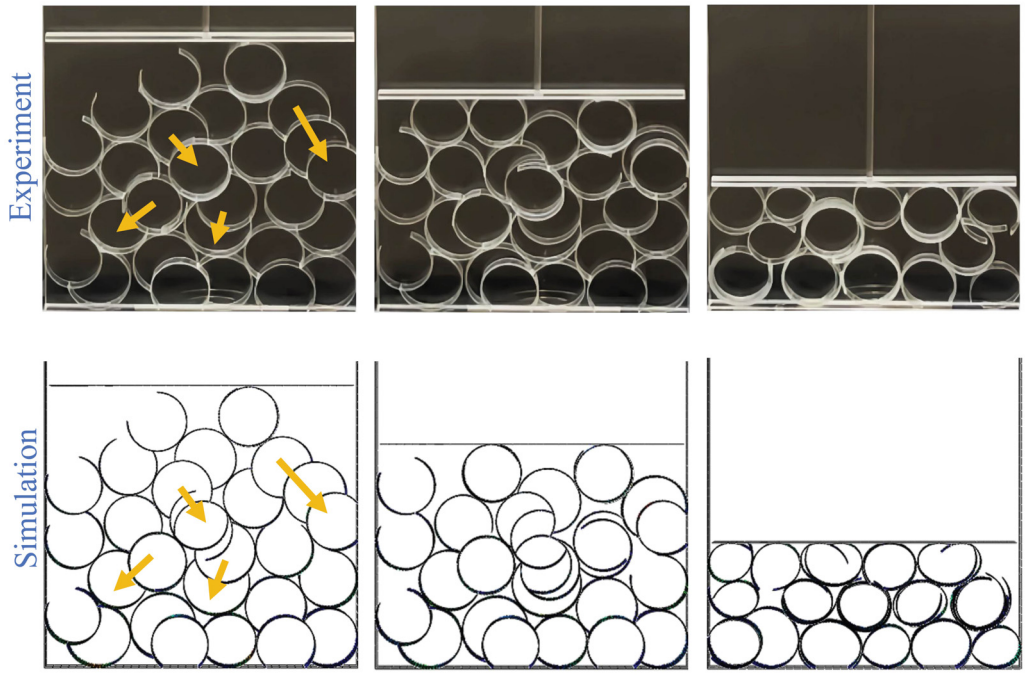

Fig. 15. Experimental and simulated deformation comparison of mechanical metamaterials composed of randomly stacked identical Type I open thin-shells.

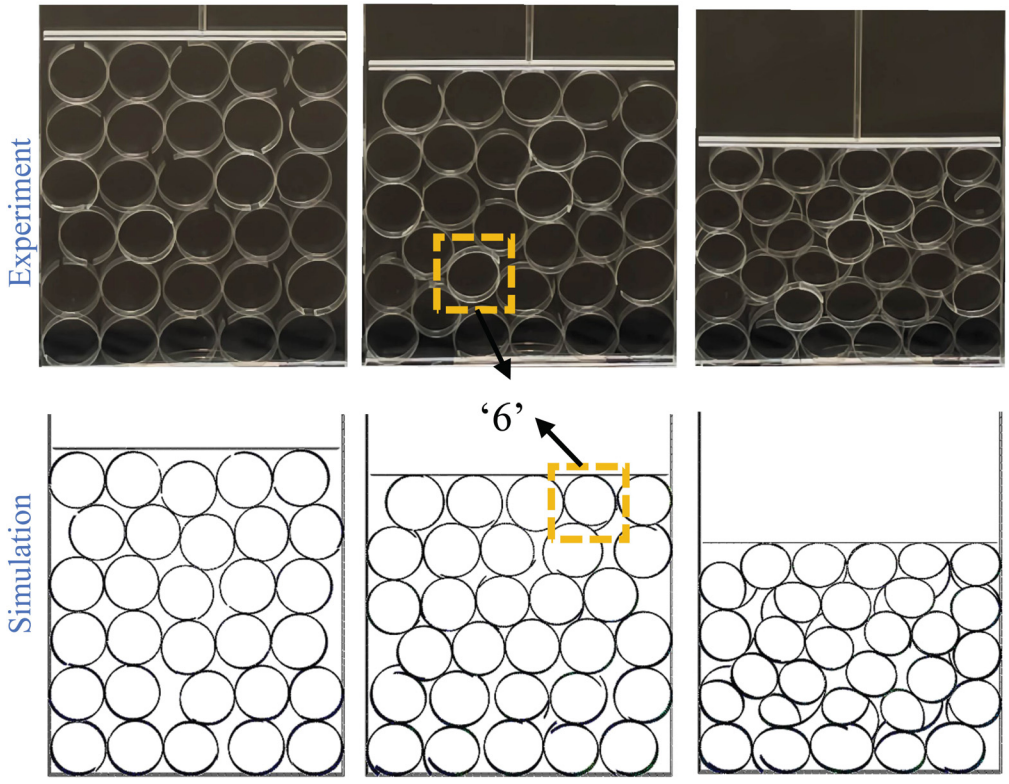

Fig. 16. Experimental and simulated deformation comparison of mechanical metamaterials composed of randomly stacked identical Type II open thin-shells.

ing configuration of these mechanical metamaterials, though slight variations exist in the internal stacking sequences between experiments and numerical simulations, both follow similar patterns. As shown in Fig. 18, we analyzed force-displacement curves at the 1st, 2nd, 5th, and 10th loading cycles to comprehensively evaluate their cyclic characteristics. The numerical simulation results are in agreement with experimental findings.

Figure 18(a1) and (a2) display experimental and numerical simulation results for mechanical metamaterials composed of randomly stacked identical Type I open thin-shells. During the first cycle, the rigid plate first moves downward, causing bending in the internal shells accompanied by an increase in F; as the rigid plate continues descending, Type I sliding snap-fit sequentially activates among the internal open thin-shells, resulting in a corresponding decrease in F, until ultimately

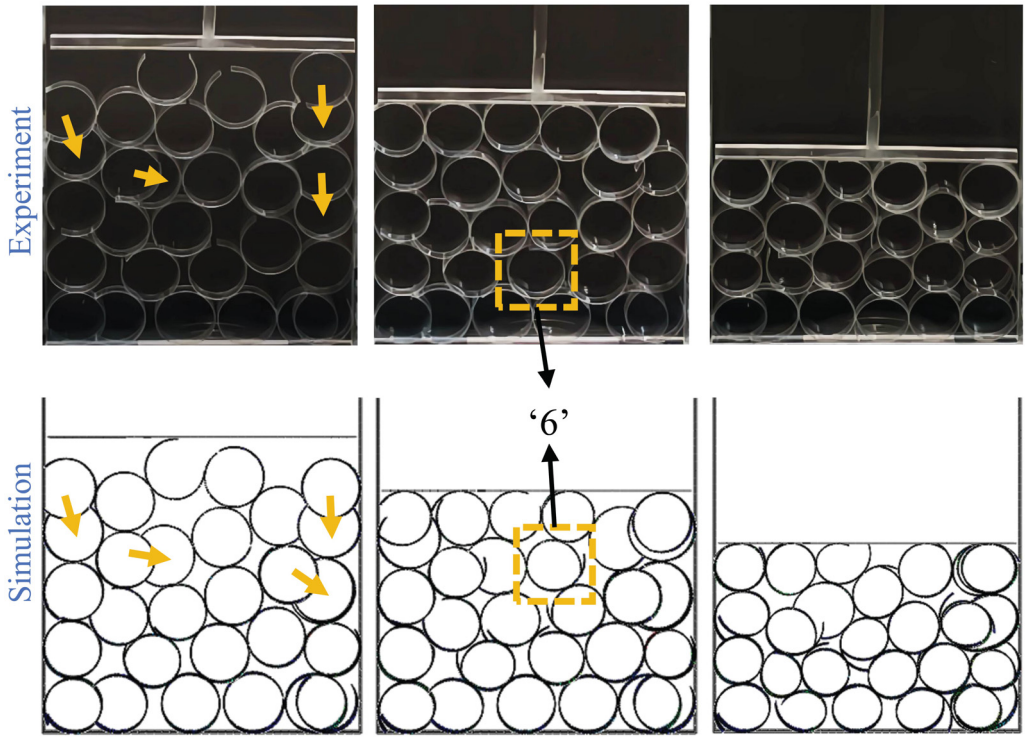

Fig. 17. Experimental and simulated deformation comparison of mechanical metamaterials with mixed random stacking of Type I and Type II open thin-shells.

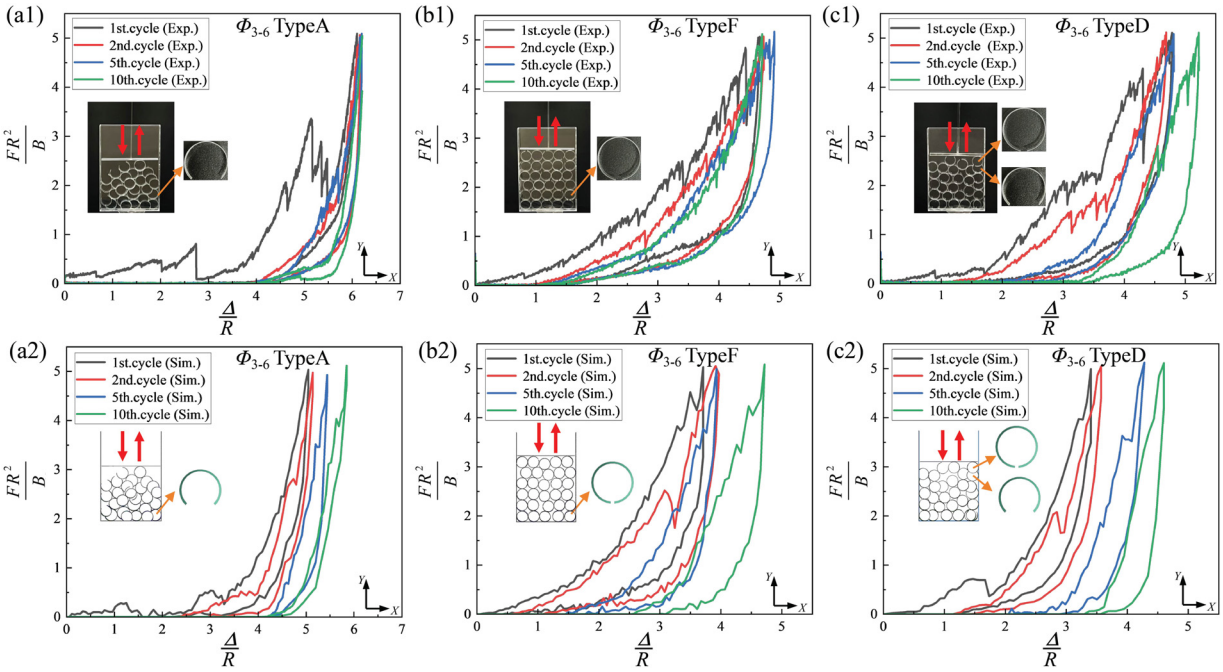

Fig. 18. Cyclic characteristics of randomly stacked mechanical metamaterials. (a1), (a2) $F-\Delta$ curves for Φ_{3-6} Type A; (b1), (b2) $F-\Delta$ curves for Φ_{3-6} Type F; (c1), (c2) $F-\Delta$ curves for Φ_{3-6} Type D.

the F rises to 5 N before the rigid plate returns to H_0. During the unloading phase, shell misfit rarely occurs. The entire compression-unloading cycle is irreversible, as the snap-fit interlocking of open thin-shells enhances the internal structural stiffness. Consequently, the stacked height of the shells becomes significantly lower than H_0. During the second cycle, the rigid plate must first descend to the stacked height of the shells at the end of the first cycle; upon contacting the shells, as bending occurs in the shells, F increases accordingly; then, as the rigid plate continues descending, a small fraction of internal open thin-shells undergo Type I sliding snap-fit, resulting in a corresponding decrease in F; ultimately, F rises to 5 N before the rigid plate returns to H_0, and the internal structural stiffness is further enhanced. During the fifth and tenth cycles, after the rigid plate descends to the surface of the stacked shells, F rapidly increases to 5 N due to compressive deformation of the shells, and the rigid plate returns to H_0, with snap-fit rarely occurring throughout the process (no significant force drop phenomenon observed). From Fig. 19(a),

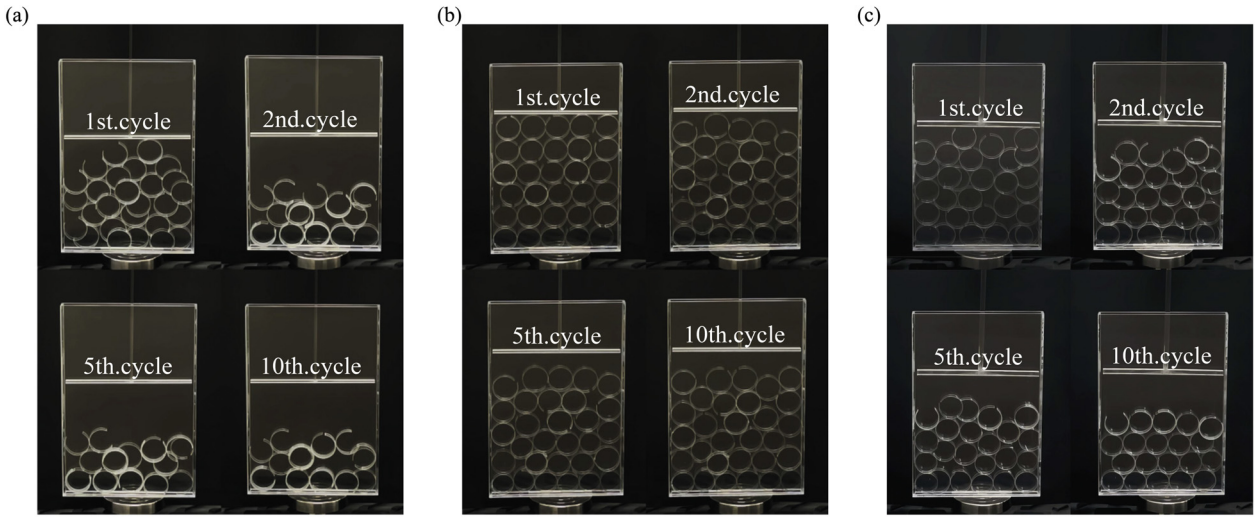

Fig. 19. Initial state before cyclic loading. (a) Φ_{3-6} Type A; (b) Φ_{3-6} Type F; (c) Φ_{3-6} Type D.

it can be observed that Type I shell snap-fit primarily occur during the first cycle, while such engagements become scarce in the second cycle; during these two cycles, the structure mainly resists compressive loading through shell snap-fit, elastic deformation, friction, and repositioning; by the fifth and tenth cycles, due to extensive snap-fit between shells, the internal stiffness of the structure has significantly increased, and compressive loading is primarily resisted through elastic deformation and friction of the shells.

Figure 18(b1) and (b2) present experimental and numerical simulation results for mechanical metamaterials composed of randomly stacked identical Type II open thin-shells. During the first cycle, the rigid plate first moves downward, causing bending in the internal shells accompanied by an increase in F; as the rigid plate continues descending, the internal Type II open thin-shells remain in a densely packed state with insufficient space for jump-type snap-fit between shells, resisting compression solely through elastic bending and large sliding deformations; ultimately, F rapidly increases to 5 N before the rigid plate returns to H_0. Although no complete shell snap-fit occurs during compression, repositioning of the shells takes place, rendering the entire compression-unloading cycle irreversible, with the stacked height of the shells now lower than H_0. During the second, fifth, and tenth cycles, after the rigid plate descends to the surface of the stacked shells, F increases to 5 N due to compressive deformation of the shells, and the rigid plate returns to H_0. Although no shell snap-fit occurs throughout the process, during each compression cycle, the shells undergo varying degrees of large deformations (e.g., coiling) due to mutual compression, causing edge-to-edge stacking of shells and a slight increase in internal structural stiffness. In every compression-unloading cycle, the structure primarily resists compressive loading through elastic deformation, friction, and repositioning of the shells. As shown in Fig. 19(b), the cyclic processes of such mechanical metamaterials exhibit relative stability.

Figure 18(c1) and (c2) present experimental and numerical simulation results for mechanical metamaterials composed of mixed randomly stacked Type I and Type II open thin-shells. During the first cycle, the rigid plate first moves downward, causing bending in the internal shells accompanied by an increase in F; as the rigid plate continues descending, sliding snap-fit occur between Type I open thin-shells and surrounding shells, resulting in a corresponding decrease in F; ultimately, F rises to 5 N before the rigid plate returns to H_0, with the snap-fit interlocking of open thin-shells enhancing the internal structural stiffness throughout this process. During the second cycle, a small number of Type I sliding snap-fit still occur; ultimately, F rises to 5 N before the rigid plate returns to H_0, and the internal structural stiffness is further enhanced. During the fifth and tenth cycles, Type I open thin-shells are virtually absent within the structure. After the rigid plate descends to the surface of the stacked shells, compression resistance is primarily achieved through large sliding deformations of Type II open thin-shells, with F increasing to 5 N due to compressive deformation of the shells before the rigid plate returns to H_0. Throughout this process, Type II open thin-shells do not actively engage in snap-fit with other shells. From Fig. 19(c), it can be observed that Type I shell snap-fit primarily occur during the first cycle, while a small number of such snap-fit also manifest in the second cycle; during these two cycles, the structure mainly resists compressive loading through shell snap-fit, elastic deformation, friction, and repositioning; by the fifth and tenth cycles, the internal stiffness of the structure has significantly increased, yet the incorporation of Type II shells relatively enhances the internal flexibility, with the structure primarily resisting compressive loading through elastic deformation, friction, and repositioning of the shells.

5.4. Mechanical properties of randomly stacked open thin-shells mechanical metamaterials under cyclic loading

In randomly stacked open thin-shell mechanical metamaterials under cyclic compression-unloading loading, snap-fit between shells are most pronounced during the first loading cycle. However, due to the randomness of initial stacking, a small number of shell snap-fit events may still be observed in the initial few cycles. This snap-fit phenomenon progressively diminishes with increasing cycle count and eventually stabilizes. Consequently, to more accurately evaluate the performance limits of such mechanical metamaterials, the tenth loading cycle is selected as limit cycle. This section focuses on investigating the mechanical performance of randomly stacked mechanical metamaterials during both the first and tenth compression-unloading cycles.

To mitigate errors arising from the initial conditions of random stacking, we conducted 30 parallel experimental trials for each of the 42 distinct configurations of randomly stacked mechanical metamaterials.

First, statistical validation of the initial stacking height H_0 of shell unit cells within the structure was performed, as shown in Fig. 20. The initial stacking height H_0 is determined by the opening angle Φ of the shells. When $\Phi \to \pi$ and Type II open thin-shells dominate numerically, the initial relative height of shell unit cells $H_0/R \to (2+6\sqrt{3})$, consistent with HCP predictions. Numerical simulation results align with experimental findings.

Subsequently, three metrics were selected to investigate the mechanical properties of randomly stacked open cylindrical thin-shell mechanical metamaterials: the maximum displacement ($\Delta_{\max}$) in a compression-unloading cycle, energy dissipation (E_{diss}) per cycle, and energy dissipa-

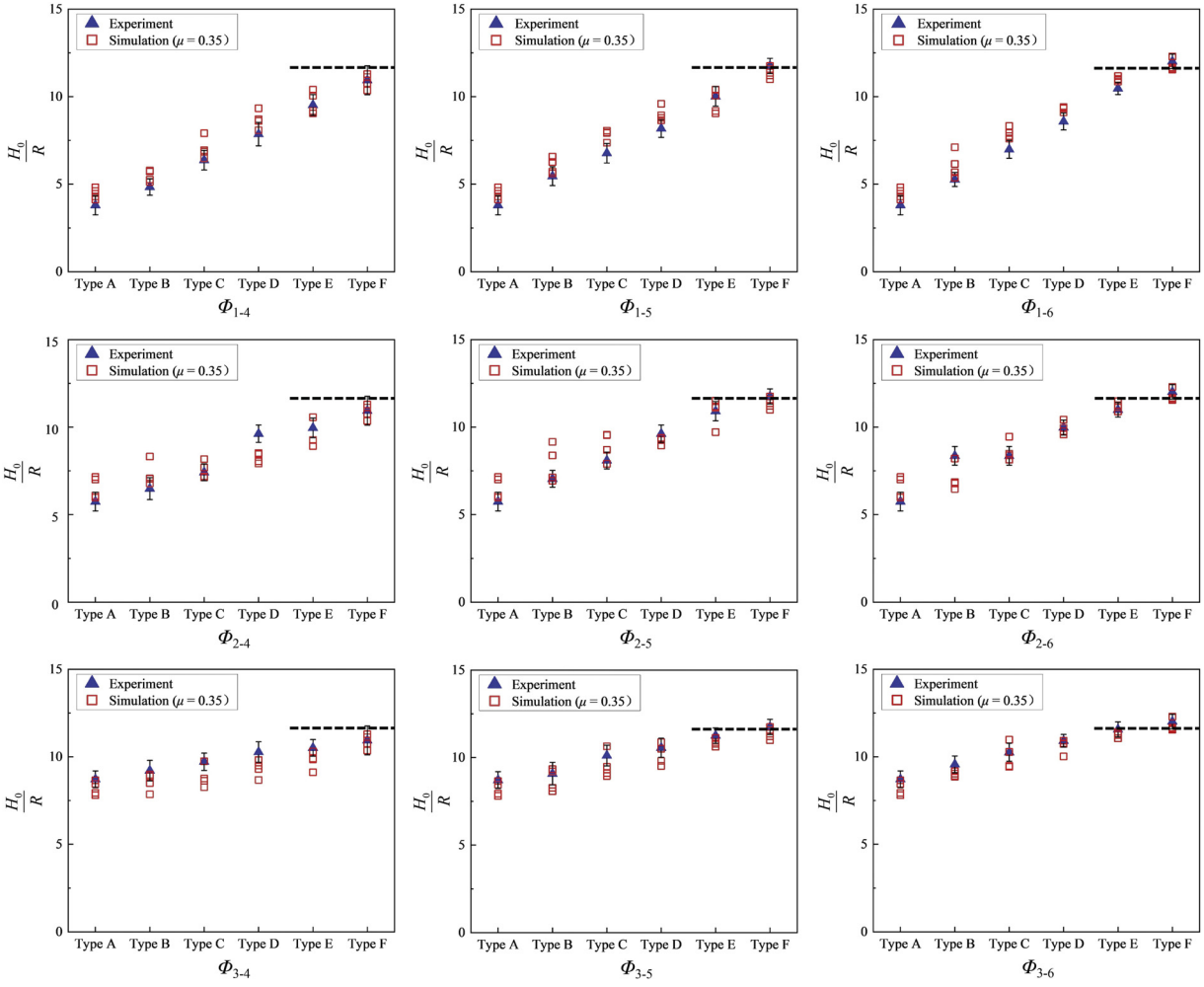

Fig. 20. Initial height H_0 of randomly stacked mechanical metamaterials under gravity (Data are presented as mean ± SD, (n = 30)).

tion ratio (η). Given the excessive number of distinct randomly stacked configurations and the substantial computational resources required for simulating limit cycles, the analysis herein primarily focuses on experimental results.

5.4.1. Comparison of maximum displacement

Maximum displacement Δ_{max} (maximum working distance) refers to the maximum deformation magnitude achieved by a structure under load, typically corresponding to the peak displacement on the force-displacement curve. It characterizes the maximum deformation level a structure can withstand under loading and serves as a critical parameter for evaluating structural performance and design safety margins. Statistical comparisons of Δ_{max} during the first and tenth cycles are presented in Fig. 21.

First, comparing Type A configurations in Fig. 21(a1), (b1), and (c1), which consist of mechanical metamaterials composed of identical Type I open thin-shells, it is observed that Δ_{max} increases with Φ. This occurs because Type I shells undergo snap-fit during compression; a larger Φ of shell requires greater snap-fit force (namely, higher assembly force f), thereby reducing the F on the rigid plate and consequently increasing the displacement required to reach the specified F_{max}. Thus, for mechanical metamaterials composed of identical Type I open thin-shells, Δ_{max} under compressive loading increases monotonically with Φ until reaching the critical angle $\Phi^*(\mu)$.

Subsequently, comparing Type F configurations in Fig. 21(a1), (a2), and (a3), which consist of mechanical metamaterials composed of identical Type II open thin-shells, it is observed that Δ_{max} remains essentially constant and exhibits minimal correlation with the opening angle Φ. This occurs because Type II shells lack sufficient space for snap-fit during compression, resisting compressive loads primarily through elastic bending and frictional sliding of the shells themselves, which exhibits minimal dependence on Φ. Type II thin-shells feature larger opening angles, enabling greater deformation and displacement under compressive forces. Thus, mechanical metamaterials composed of Type II thin-shells demonstrate exceptional flexibility, achieving substantial displacements during compression while maintaining structural stability.

Next, comparing the four configurations—Type B, Type C, Type D, and Type E—in Fig. 21(a1), which consist of mechanical metamaterials composed of mixed Type I and Type II open thin-shells, it is observed that Δ_{max} increases with the rising proportion of Type II open thin-shells in the mixture. This occurs because the incorporation of Type II shells enhances the structural flexibility, enabling the system to withstand greater deformation while maintaining substantial stability.

Finally, comparing the four configurations–Type B, Type C, Type D, and Type E—in Fig. 21(a1), (b1), and (c1), which consist of mechanical metamaterials composed of mixed Type I and Type II open thin-shells, it is observed that Δ_{max} increases with the rising Φ of Type I open thin-shells in the mixture. This occurs because a larger Φ of Type I shells requires greater assembly force, resulting in a reduced F on the rigid plate and thereby increasing the displacement required to reach the specified F_{max}.

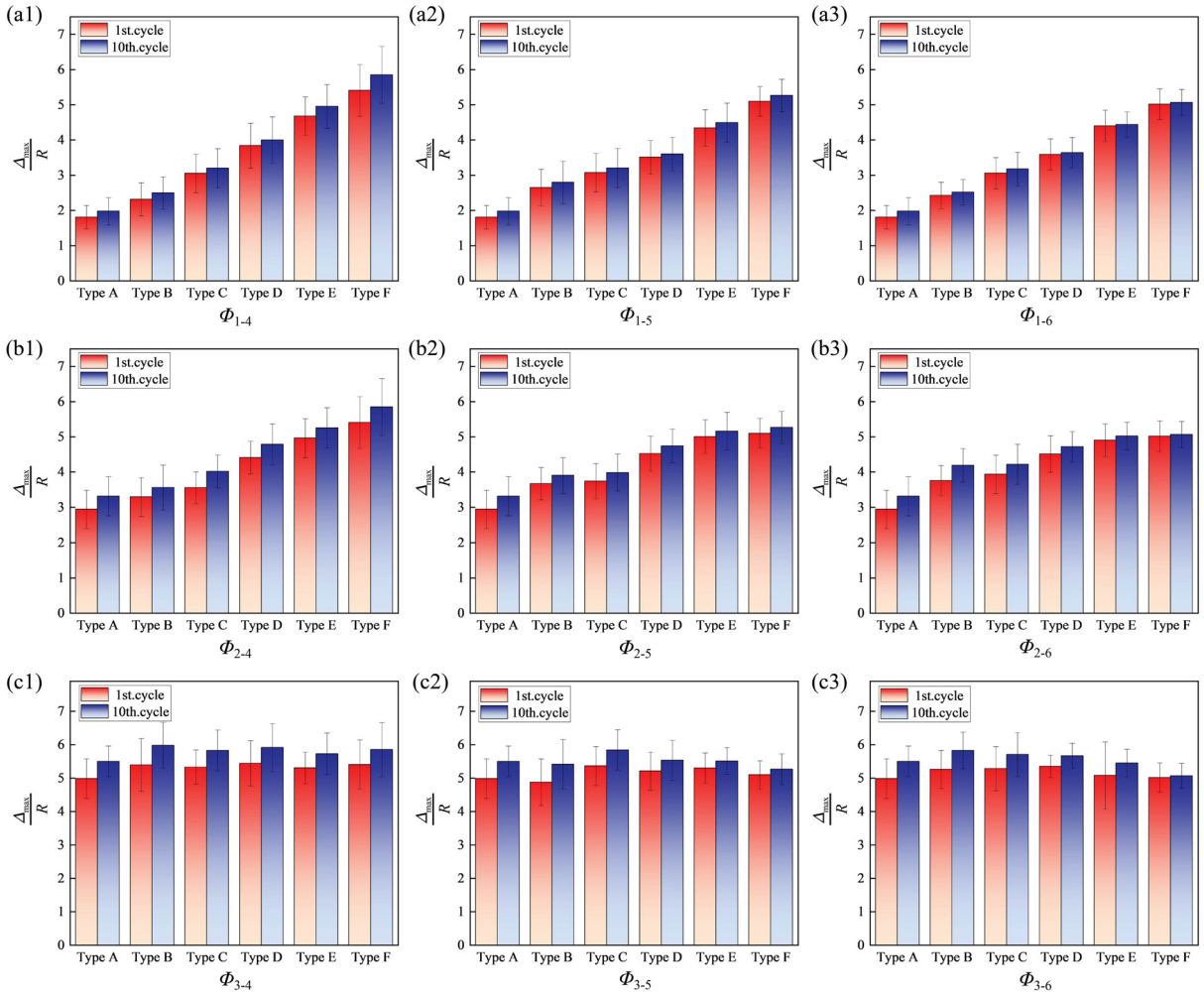

Fig. 21. Comparison of maximum displacement (Δ_{max}) at the first and tenth cycles. (a1)–(a3) Open thin-shell mechanical metamaterials composed of Φ_1 shells randomly stacked with Φ_4, Φ_5, and Φ_6 shells in different proportions, respectively; (b1)–(b3) open thin-shell mechanical metamaterials composed of Φ_2 shells randomly stacked with Φ_4, Φ_5, and Φ_6 shells in different proportions, respectively; (c1)–(c3) open thin-shell mechanical metamaterials composed of Φ_3 shells randomly stacked with Φ_4, Φ_5, and Φ_6 shells in different proportions, respectively. (Data are presented as mean ± SD, (n = 30)).

From the perspective of Δ_{max}, whether in the first cycle or the tenth cycle, larger Φ of shell unit cells in randomly stacked mechanical metamaterials yield enhanced composite effectiveness and superior structural performance, with the Δ_{max} reaching 5–6 times the shell unit cell radius R.

5.4.2. *Comparison of energy dissipation*

This analysis primarily focuses on energy dissipation E_{diss} induced by damping effects. The energy dissipation per compression-unloading cycle can be calculated as the area enclosed by the force-displacement curve, namely

$$E_{diss} = \oint F \mathrm{d}\Delta, \tag{3}$$

where F denotes the load value on the rigid plate, and Δ represents the displacement of the rigid plate.

The energy dissipation capacity of a structure serves as a critical parameter for evaluating its performance under cyclic loading, with significant implications for enhancing structural stability and durability. Statistical comparisons of E_{diss} during the first and tenth cycles are presented in Fig. 22.

First, comparing Type A configurations in Fig. 22(a1), (b1), and (c1), which consist of mechanical metamaterials composed of identical Type I open thin-shells, during the first cycle, E_{diss} increases with the Φ. At this stage, Type I shells undergo snap-fit during compression; a larger Φ requires greater snap-fit force, resulting in reduced F on the rigid plate and consequently increasing the displacement required to reach the specified F_{max}. During unloading, Type I shells exhibit virtually no mismatch phenomena. Thus, E_{diss} throughout the cycle is predominantly governed by the compression process. By the tenth cycle, shell unit cells capable of snap-fit engagements within the structure have completed, and the superposition effect of multi-layered shells enhances structural stiffness, leading to minimal variation in E_{diss} per cycle. In summary, for mechanical metamaterials composed of identical Type I open thin-shells under cyclic loading, E_{diss} increases monotonically with Φ during the first cycle until reaching the critical angle $\Phi^*(\mu)$; whereas at the tenth cycle, E_{diss} may be regarded as constant.

Subsequently, comparing Type F configurations in Fig. 22(a1), (a2), and (a3), which consist of mechanical metamaterials composed of identical Type II open thin-shells, during the first cycle, E_{diss} exhibits minimal variation and is essentially independent of the Φ. This occurs because, although the Φ of Type II shells differ during the first cycle, frictional contacts and repositioning between shells have not yet fully developed; consequently, E_{diss} is primarily determined by elastic deformation of the shells and minor frictional dissipation, resulting in negligible differences in E_{diss}. By the tenth cycle, the structure has undergone multiple compression-unloading processes, with cumulative inter-shell contacts and friction. Shells with larger Φ develop greater contact areas

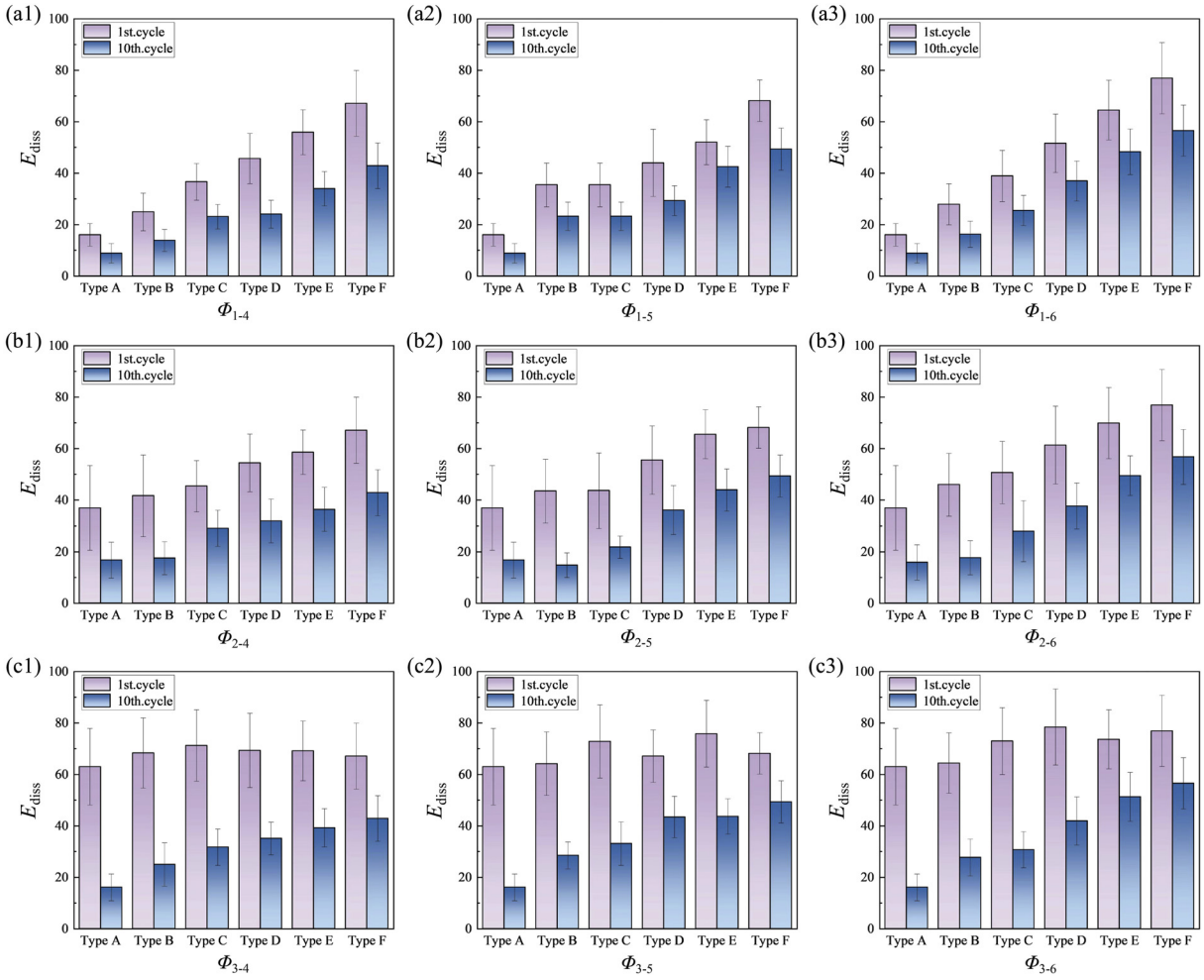

Fig. 22. Comparison of energy dissipation(E_{diss}) at the first and tenth cycles. (a1)–(a3) Open thin-shell mechanical metamaterials composed of Φ_1 shells randomly stacked with Φ_4, Φ_5, and Φ_6 shells in different proportions, respectively; (b1)–(b3) open thin-shell mechanical metamaterials composed of Φ_2 shells randomly stacked with Φ_4, Φ_5, and Φ_6 shells in different proportions, respectively; (c1)–(c3) open thin-shell mechanical metamaterials composed of Φ_3 shells randomly stacked with Φ_4, Φ_5, and Φ_6 shells in different proportions, respectively. (Data are presented as mean ± SD, (n = 30)).

during compression, generating stronger frictional forces that increase E_{diss}. Thus, for mechanical metamaterials composed of identical Type II open thin-shells under cyclic loading, E_{diss} may be considered constant during the first cycle, whereas at the tenth cycle, E_{diss} increases monotonically with Φ.

Next, comparing the four configurations—Type B, Type C, Type D, and Type E—in Fig. 22(a1), which consist of mechanical metamaterials composed of mixed Type I and Type II open thin-shells, E_{diss} increases with the rising proportion of Type II open thin-shells during both the first and tenth loading cycles. This behavior is attributed to the enhanced structural flexibility resulting from the incorporation of Type II shells, thus strengthening the energy dissipation capacity of the structure.

Finally, comparing the four configurations—Type B, Type C, Type D, and Type E—in Fig. 22(a1), (b1), and (c1), which consist of mechanical metamaterials composed of mixed Type I and Type II open thin-shells, during the first cycle, E_{diss} increases with the rising Φ of Type I open thin-shells in the mixture. At the tenth cycle, E_{diss} exhibits minimal variation. This behavior arises because larger Φ of Type I shells dissipate more energy during compression, whereas during unloading, shells exhibit no misfit.

From the perspective of E_{diss}, whether in the first cycle or the tenth cycle, larger Φ of shell unit cells in randomly stacked mechanical metamaterials significantly enhance the energy dissipation capacity under cyclic loading, achieving a fivefold enhancement.

5.4.3. Comparison of energy dissipation ratio

The energy dissipation ratio η is defined as the ratio of energy utilized for useful work to the total input energy during a single cycle. The calculation formula for η is

$$\eta = \frac{E_{diss}}{E_{in}}, \tag{4}$$

where E_{diss} is the energy dissipated during that cycle, and $E_{in} = F_{max}\Delta_{max}$ is the total energy input per compression-unloading cycle.

The energy dissipation ratio η of a structure reflects the effectiveness of energy utilization from the input energy and serves as a key metric for evaluating structural energy performance. Statistical comparisons of η during the first and tenth cycles are presented in Fig. 23.

Comparing η during the first cycle of randomly stacked mechanical metamaterials, it is observed that no significant correlation exists between η and Φ, with η exhibiting minimal variation and may be regarded as constant. This indicates that during the initial cycle, the structure demonstrates robust stability and reliability in terms of energy utilization efficiency and overall performance.

Comparing η during the tenth cycle of randomly stacked mechanical metamaterials, it is observed that larger Φ of shell unit cells in randomly stacked mechanical metamaterials yield higher η.

From the perspective of η, under a single compression-unloading cycle, randomly stacked mechanical metamaterials with different open thin-shell configurations exhibit essentially constant η values, indicat-

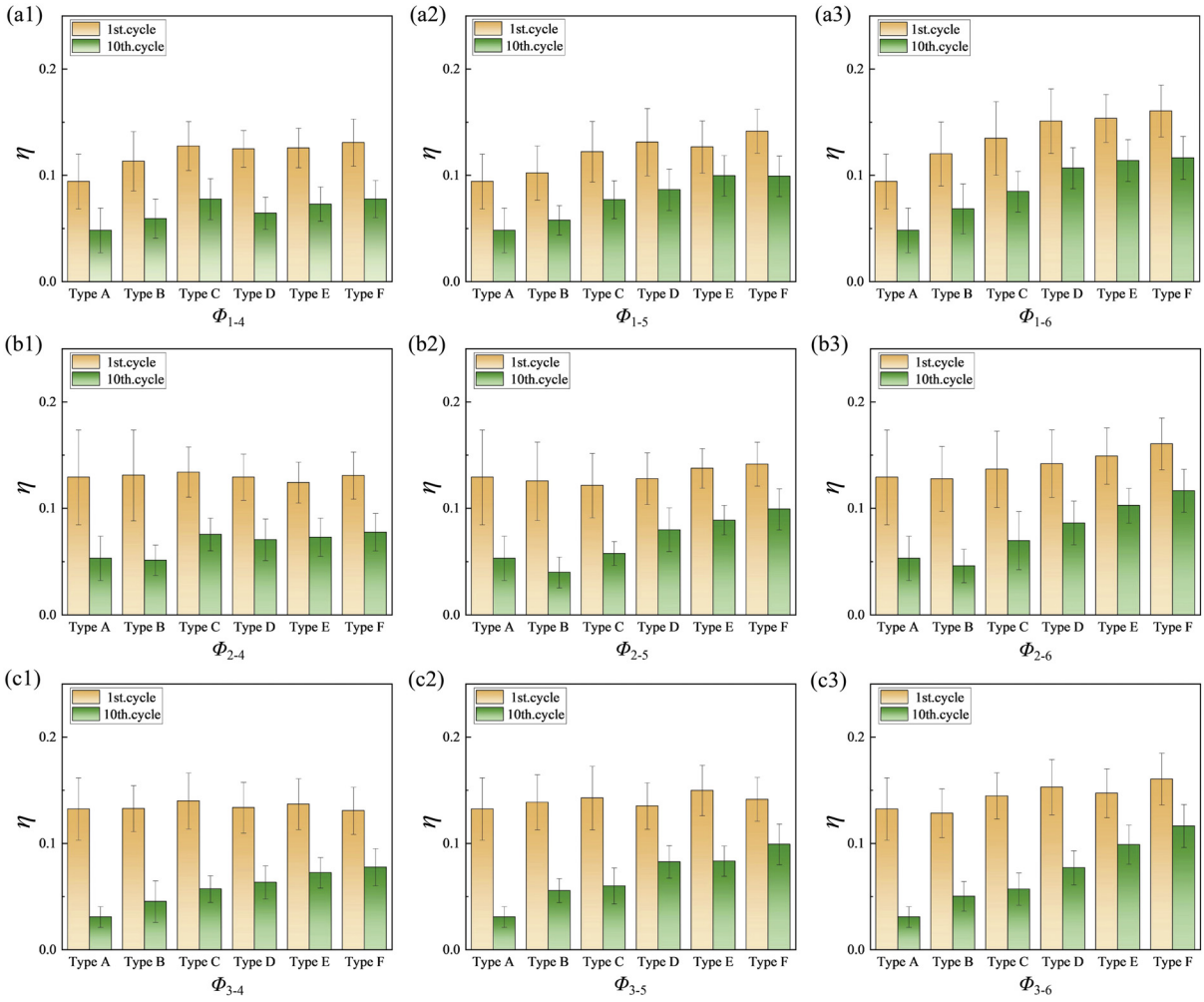

Fig. 23. Comparison of energy dissipation ratio (η) at the first and tenth cycles. (a1)–(a3) Open thin-shell mechanical metamaterials composed of Φ_1 shells randomly stacked with Φ_4, Φ_5, and Φ_6 shells in different proportions, respectively; (b1)–(b3) open thin-shell mechanical metamaterials composed of Φ_2 shells randomly stacked with Φ_4, Φ_5, and Φ_6 shells in different proportions, respectively; (c1)–(c3) open thin-shell mechanical metamaterials composed of Φ_3 shells randomly stacked with Φ_4, Φ_5, and Φ_6 shells in different proportions, respectively. (Data are presented as mean ± SD, (n = 30)).

ing exceptional performance stability. Under cyclic loading, larger Φ of shell unit cells in randomly stacked mechanical metamaterials yield progressively higher η values, thereby enhancing structural reliability and stability.

6. Conclusions

This study designed and fabricated 42 distinct configurations of randomly stacked mechanical metamaterials composed of open thin-shells. Employing a combined experimental and numerical simulation approach, the mechanical properties and energy dissipation of two thin-shell unit cells under compressive loading were first analyzed. Building on this foundation, the investigation further examined the deformation processes under compressive loading, cyclic characteristics under cyclic loading, and mechanical performance of randomly stacked thin-shells metamaterials with varying configurations. The principal conclusions are summarized as follows:

(1) Through experimental and numerical simulation studies on two cylindrical open thin-shell unit cells, it was found that Type II shells demonstrate superior energy dissipation performance, exhibiting 40 to 50 times higher energy dissipation capacity compared to Type I shells. Guided by structural energy absorption principles, high-efficiency energy dissipation in Type II shells can be achieved via synergistic optimization of the opening angle Φ and friction coefficient μ.

(2) Through investigation of deformation processes in randomly stacked open thin-shells mechanical metamaterials under compressive loading, it was found that regardless of configuration, in close-packed assemblies of shell unit cells, Type I shells readily undergo snap-fit, while Type II shells, constrained by surrounding shells, resist compression exclusively through their own elastic bending and friction without actively initiating snap-fit. During compression, shell unit cells dissipate energy through large deformations, snap-fit, friction, and repositioning.

(3) Through investigation of the dynamic characteristics of randomly stacked open thin-shells mechanical metamaterials under cyclic loading, it was found that metamaterials composed of identical Type II open thin-shells in random stacking configurations exhibit superior stability.

(4) Through investigation of the mechanical performance of randomly stacked open thin-shells mechanical metamaterials under cyclic loading, it was found that with increasing opening angle Φ of Type I shells, the maximum displacement and energy dissipation capacity of the structure increase progressively until reaching the critical angle $\Phi^*(\mu)$. When shells are mixed in stacking configurations, increasing the proportion of Type II thin-shells significantly enhances the overall flexibility of the structure. This

enhancement enables the structure to achieve greater displacement and energy dissipation under compressive loading without compromising its stability.

(5) During the first compression-unloading cycle, the energy dissipation ratio η remains virtually identical across different configurations of randomly stacked mechanical metamaterials, indicating that the energy dissipation efficiency exhibits robust stability independent of contact and geometric randomness. However, at limit cycles, Type II-dominant metamaterials achieve higher η values, demonstrating their superior structural attributes.

Declaration of competing interest

The authors declare that they have no known competing financial interests or personal relationships that could have appeared to influence the work reported in this paper.

CRediT authorship contribution statement

Xiaolin Guo: Writing – review & editing, Writing – original draft, Visualization, Validation, Software, Resources, Project administration, Methodology, Investigation, Formal analysis, Data curation. **Bohua Sun:** Writing – review & editing, Writing – original draft, Validation, Supervision, Resources, Formal analysis, Data curation, Conceptualization.

References

[1] J. Sun, J. Zhou, Metamaterials: the art in materials science, Engineering 44 (2024) 145–161.
[2] J. Gu, W. Zhap, C. Zeng, L. Liu, J. Leng, Y. Liu, Construction of mechanical metamaterials and their extraordinary functions, Compos. Struct. 356 (2025) 118872.
[3] J.E. Holliman, H.T. Schaef, B.P. McGrail, Q.R.S. Miller, Review of foundational concepts and emerging directions in metamaterial research: design, phenomena, and applications, Mater. Adv. 3 (2022) 8390–8406.
[4] L. Wu, X. Xi, B. Li, J. Zhou, Multi-stable mechanical structural materials, Adv. Eng. Mater. 20 (2018) 1700599.
[5] M.J. Islam, B. Bao, F. Peng, Recent developments of mechanical metamaterials inspired by origami: from methodologies, fabrication to challenges, Appl. Mater. Today 44 (2025) 102715.
[6] Y. Wang, L. Liu, D. Hofmann, J.E. Andrade, C. Daraio, Structured fabrics with tunable mechanical properties, Nature 596 (2021) 238–243.
[7] Y. Gao, X. Kang, B. Li, Programmable mechanical metamaterials with tunable poisson's ratio and morphable stiffness, Compos. Part B-Eng. 292 (2025) 112089.
[8] L. Zhang, S. Yan, W. Liu, Y. Liu, W. Cai, Z. Zhang, J. Zhou, Mechanical metamaterials with negative poisson's ratio: a review, Eng. Struct. 329 (2025) 119838.
[9] N.V. Viet, W. Zaki, On exploration of directional extreme mechanical attributes and energy absorption of bending-dominated and buckling-induced negative Poisson's ratio metamaterials, Compos. Struct. 349 (2024) 118460.
[10] M. Noda, T. Yamada, Quasi-isotropic metamaterials with negative thermal expansion designed topology optimization using topological derivative, Compos. Struct. 365 (2025) 365.
[11] C. Liu, X. Zhang, J. Chang, L. You, J. Zhao, S. Qiu, Programmable mechanical metamaterials: basic concepts, types, construction strategies-a review, Front. Mater. 11 (2024) 1361408.
[12] W. Liu, H. Jiang, Y. Chen, 3D programmable metamaterials based on reconfigurable mechanism modules, Adv. Funct. Mater. 32 (2022) 2109865.
[13] S. Yan, L. Wu, Y. Wen, J. Sun, J. Zhou, Snap-through instability in mechanical metamaterials, Responsive Mater. 3 (2025) e20240035.
[14] B. Jiang, X. Chen, J. Yu, Y. Zhao, Z. Xie, H. Tan, Energy-absorbing properties of thin-walled square tubes filled with hollow spheres, Thin. Wall. Struct. 180 (2022) 109765.
[15] J. Lu, Q. Li, R. Qin, X. Wang, T. Li, H. Niu, B. Chen, Enhanced energy absorption of assembled honeycomb system under in-plane compression, In. J. Mech. Sci. (2025) 110404.
[16] Z. Yu, R. Savinov, M. Matura, P. Zhang, J. Shi, Current research status on advanced lattice structures for impact and energy absorption applications: a systematic review, Thin. Wall. Struct. 215 (2025) 113490.
[17] K. Fu, Z. Zhao, L. Jin, Programmable granular metamaterials for reusable energy absorption, Adv. Funct. Mater. 29 (2019) 1901258.
[18] S. Yan, Z. Meng, W. Liu, X. Tan, P. Cao, Y. Wen, Z. Xiang, J. Chen, Y. Xu, Y. Wang, J. Sun, L. Wu, J. Zhou, Self-contact snapping metamaterial for tensile energy dissipation, Mater. Horiz. 11 (2024) 6352–6360.
[19] J. Hua, Y. Zhou, Z. Meng, C. Chen, Pre-compressed beam-based multistable mechanical metamaterials with programmable loading and unloading deformation sequences, Thin. Wall. Struct. 209 (2025) 112879.
[20] K. Bertoldi, V. Vitelli, J. Christensen, M.V. Hecke, Flexible mechanical metamaterials, Nat. Rev. Mater. 2 (2017) 1–11.
[21] F. Liu, T. Terakawa, J. Lin, M. Komori, Design of modular deployable structure with programmable multistability, In. J. Mech. Sci. 288 (2025) 110037.
[22] A. Rafsanjani, A. Akbarzadeh, D. Pasini, Snapping mechanical metamaterials under tension, Adv. Mater. 27 (2015) 5931–5935.
[23] R. Xu, Y. He, X. Li, M. Lu, Y. Chen, Snap-fit mechanical metamaterials, Appl. Mater. Today 30 (2023) 101714.
[24] R. Xu, Y. He, C. Chen, J. Sun, X. Li, M. Lu, Y. Chen, Rotation-based snap-fit mechanical metamaterials, Adv. Sci. 12 (2025) 2501749.
[25] P.M. Reis, A perspective on the revival of structural (in) stability with novel opportunities for function: from buckliphobia to buckliphilia, J. Appl. Mech. 82 (2015) 111001.
[26] T.G. Sano, T. Yamaguchi, H. Wada, Slip morphology of elastic strips on frictional rigid substrates, Phys. Rev. Lett. 118 (2017) 178001.
[27] P. Grandgeorge, T.G. Sano, P.M. Reis, An elastic rod in frictional contact with a rigid cylinder, J. Mech. Phys. Solids 64 (2022) 104885.
[28] T.G. Sano, H. Wada, Snap-buckling in asymmetrically constrained elastic strips, Phys. Rev. E 97 (2018) 013002.
[29] K. Yoshida, H. Wada, Mechanics of a snap fit, Phys. Rev. Lett. 125 (2020) 194301.
[30] X.L. Guo, B.H. Sun, Assembly and disassembly mechanics of a spherical snap fit, Theor. Appl. Mech. Lett. 13 (2023) 100403.
[31] X.L. Guo, B.H. Sun, Mechanics of a thin-walled segmented torus snap fit, Thin. Wall. Struct. 198 (2024) 111676.
[32] X.L. Guo, B.H. Sun, Detachable connection mechanics of thin-walled cylindrical snap fit docking, Extreme Mech. Lett. 67 (2024) 102122.
[33] K. Yoshida, H. Wada, Indentation of an elastic arch on a frictional substrate: pinning, unfolding, and snapping, Phys. Rev. E 109 (2024) 045001.
[34] C. Poirier, M. Ammi, D. Bideau, J.P. Troadecl, Experimental study of the geometrical effects in the localization of deformation, Phys. Rev. Lett. 68 (1992) 216.
[35] S. Poincloux, T. Chen, B. Audoly, P.M. Reis, Bending response of a book with internal friction, Phys. Rev. Lett. 126 (2021) 218004.
[36] B.H. Sun, W. Dang, X.T. Liu, X.L. Guo, Bending response and energy dissipation of interlayer slidable friction booklike-plates, Acta Mech. Sinica 39 (2023) 222449.
[37] M. Zaiser, S. Zapperi, Disordered mechanical metamaterials, Nat. Rev. Phys. 5 (2023) 679–688.
[38] D. Tuzes, P.D. Ispnovity, M. Zaiser, Disorder is good for you: the influence of local disorder on strain localization and ductility of strain softening materials, Int. J. Fract. 205 (2017) 139–150.
[39] L. Liu, B. Xia, Y. Zhou, K. Wei, Disordered mechanical metamaterials with programmable properties, Acta Mater. 285 (2025) 120700.
[40] T.G. Sano, E. Hohnadel, T. Kawata, T. Metivet, F. Bertails-Descoubes, Randomly stacked open cylindrical shells as functional mechanical energy absorber, Commun. Mater. 4 (2023) 59.
[41] A. Thue, Om nogle geometrisk-taltheoretiske theoremer, Forandlingerneved de Skandinaviske Naturforskeres 14 (1892) 352–353.